

# POLYMORPHISM OF TRICALCIUM SILICATE IN PORTLAND CEMENT: A FAST VISUAL IDENTIFICATION OF STRUCTURE AND SUPERSTRUCTURE.

M. Courtial <sup>a</sup>, M.-N. de Noirfontaine <sup>b,c</sup>, F. Dunstetter <sup>b</sup>, G. Gasecki <sup>c</sup>, M. Signes-Frehel <sup>c</sup>

<sup>a</sup> Laboratoire d'Artois Mécanique et Habitat, Université d'Artois, route de l'Université 62408 Béthune, France

<sup>b</sup> Laboratoire des Solides Irradiés, Ecole Polytechnique, 91128 Palaiseau Cedex, France

<sup>c</sup> CTG, Ciments CALCIA-Italcementi Group, rue des Technodes, 78931 Guerville Cedex, France

## Abstract

So-called alite is a solid solution of tricalcium silicate  $\text{Ca}_3\text{SiO}_5$  with a few percent of impurities. It constitutes the major phase of anhydrous Portland cement. In industrial compounds, alite crystallises into two monoclinic forms designated M1 and M3. The possibility of correlation between the crystallographic structure of the clinker and its reactivity is still an open question. The answer of such a question involves a proper quantitative analysis of the various phases –including the exact alite polymorph- of the industrial product.

The rather similar structure of the two alites makes it difficult to distinguish them from their XRD patterns. This paper shows that five angular windows in the X-Ray diffraction patterns can be used with synthetic alites as well as industrial compounds, to identify the nature of the actual polymorph (M1 or M3) present and the structural model to be used (with or without superstructure) in subsequent Rietveld analysis of the data.

Keywords: anhydrous cement, polymorphism, superstructure, X-Ray powder diffraction.

# **POLYMORPHISM OF TRICALCIUM SILICATE IN PORTLAND CEMENT: A FAST VISUAL IDENTIFICATION OF STRUCTURE AND SUPERSTRUCTURE.**

M. Courtial <sup>a</sup>, M.-N. de Noirfontaine <sup>b,c</sup>, F. Dunstetter <sup>b</sup>, G. Gasecki <sup>c</sup>, M. Signes-Frehel <sup>c</sup>

*a Laboratoire d'Artois Mécanique et Habitat, Université d'Artois, route de l'Université 62408 Béthune, France*

*b Laboratoire des Solides Irradiés, Ecole Polytechnique, 91128 Palaiseau Cedex, France*

*c CTG, Ciments CALCIA-Italcementi Group, rue des Technodes, 78931 Guerville Cedex, France*

## **Introduction**

Firing a mixture of limestone and clay in a cement kiln at about 1450° C produces an artificial rock-like material known as clinker which is the main constituent (some 90 to 95 wt. %) of anhydrous Portland cement.

Clinker itself is a mixture of at least four distinct compounds. Large crystals of alite and belite, which are the industry designations for tricalcium and dicalcium silicate respectively, normally stabilised with some impurity elements, are embedded in an interstitial phase made of a mixture of tricalcium aluminate and calcium alumino-ferrite phases. All phases exhibit a more or less complex polymorphism depending on the nature of impurities and the thermal parameters of the process (temperature of the kiln and cooling rate). The origin of the impurities depends on the composition of the minerals in the quarry and the nature of the fuel.

Alite is the major phase (between 50 and 70 % of clinker). Seven polymorphs are known: three triclinic polymorphs T1, T2, T3, three monoclinic M1, M2, M3, and a rhombohedral high temperature polymorph R. The M3 polymorph is not found in pure tricalcium silicate. In industrial clinkers, the M1 and M3 polymorphs are mostly stabilised at room temperature by the presence of sulfate or magnesium impurities respectively (Maki and Goto 1982): these clinkers will be hereafter referred to as M1-type and M3-type clinkers.

This paper aims at showing the signatures of the monoclinic forms on the X-Ray diffraction patterns. We will describe successively the synthetic alite and the real industrial clinkers.

## 1. Synthetic alites M1, M2, M3.

### Experimental.

M1 and M2 alites have been synthesised using the conditions described in Qing et al. (1992), and M3 alite on the basis of the formulation of Regourd (Guinier and Regourd 1969). Their chemical compositions (wt. %) determined by X-Ray fluorescence are given in Table 1.

Fig. 1 shows the three X-Ray diffraction patterns carried out with the same conditions. Each sample was ground in an agate mortar and was passed through a 40  $\mu\text{m}$  sieve with 0 % retained. A Philips PW 1050/70 X-ray powder diffractometer was used, with Bragg Brentano geometry,  $\text{CuK}\alpha$  radiation (40kV, 30 mA) and graphite post-diffraction monochromator (divergence slit =  $1^\circ$ , receiving slit = 0.1 mm, scatter slit =  $1^\circ$ ). The data were collected from  $2\theta = 10^\circ$  to  $80^\circ$ , using a step interval of  $0.02^\circ$ , and a step counting time of 10s.

### Angular windows versus structural models.

Initially, the X-Ray diffraction patterns look rather similar, but the use of five angular windows in the diffraction patterns (referred to as W1 to W5 hereafter) is sufficient to distinguish between them. These five angular windows are defined in Table 2 and Fig. 2. The indices of the Bragg lines or group of Bragg lines are given by Table 2. Various indices corresponding to various structural models used in this paper are given together with the pseudo-orthohexagonal indices from the literature.

Several unit cells can be used to describe the three alites. Pseudo-orthohexagonal unit cells (built on the two diagonals of the basis of the pseudo-hexagonal unit cells) were introduced at the very beginning in the first systematic powder diffraction study of Regourd and co-workers (Bigare et al. 1967, Guinier et al. 1969, Regourd 1979), hereafter referred to as  $\text{OH}_1$ ,  $\text{OH}_2$  and  $\text{OH}_3$ . For the M1 and M3 alites, monoclinic structural models are known (M1: de Noirfontaine 2000; M3: Nishi et al. 1985 and Mumme 1995) hereafter referred to as M1,  $\langle\text{M}\rangle_1$ , M3 and  $\langle\text{M}\rangle_3$ . Here  $M_n$  and  $\langle\text{M}\rangle_n$  stand for the unit cell respectively with and without superstructure: the M1 and M3 unit cells are respectively 3 times and 6 times larger than the  $\langle\text{M}\rangle_1$  and  $\langle\text{M}\rangle_3$  unit cells. The unit cell parameters refined for our samples are given in Table 3 (footnote 1) with experimental errors. The Rietveld refinements (Rietveld 1969) were carried out using Fullprof (Rodriguez 1994) and GSAS (Larson and Von Dreele 1988) softwares. The other unit cells are computed using transformation matrices (de Noirfontaine 2000). We use non-conventional  $\langle\text{M}\rangle$  unit cells in order to

evidence the superstructure relations with the  $M'$  unit cells equivalent to the  $M$  unit cells: the various cell choices of the monoclinic unit cells are defined in International Tables of Crystallography. As sketched in Fig. 3, they are related to a circular permutation of the  $a$  and  $c$  unit cell vectors in the monoclinic plane.

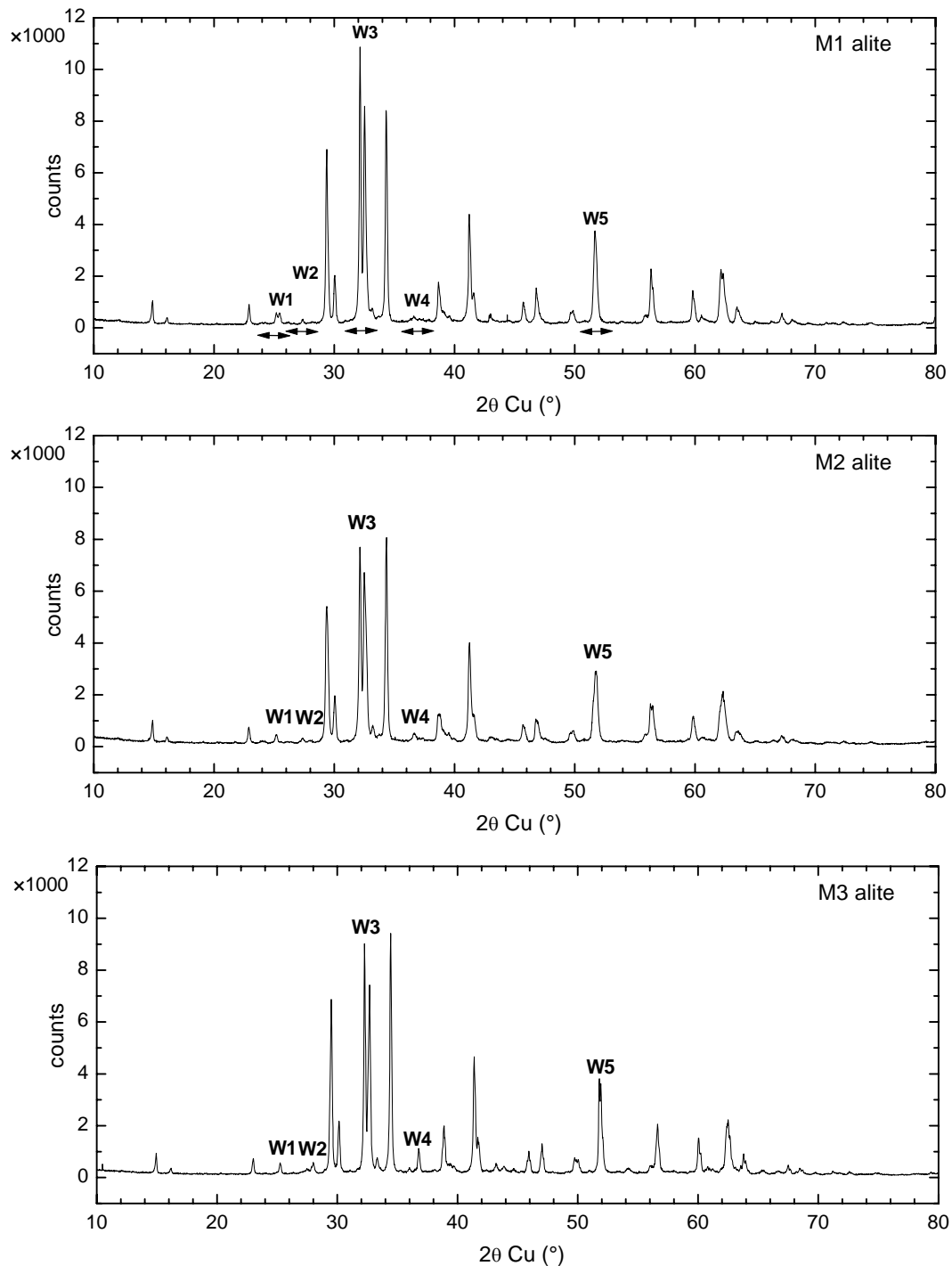


Fig. 1. Powder X-Ray diffraction patterns of three synthetic alites M1, M2, and M3.

The M3 alite is stabilised by MgO impurities. In this case, one observes either the M3 structure determined by Nishi on a synthetic alite (Nishi et al. 1985) or the six time smaller unit cell  $\langle M \rangle_3$  observed by Mumme. The superstructure relation between these two unit cells is described by Nishi (1985). The M1 alite is

stabilised by sulfate impurities (Maki and Goto 1982). We have studied synthetic alite (de Noirfontaine 2000) and interpreted it as a 3-fold superstructure of an average unit cell here referred to as  $\langle M \rangle_1$ . It is rather similar to the  $\langle M \rangle_3$  Mumme (1995) unit cell, but with a different space group (Pc instead of Cm).

Since no atomic model is known for the M2 polymorph, an average  $\langle M \rangle$  unit cell is used.

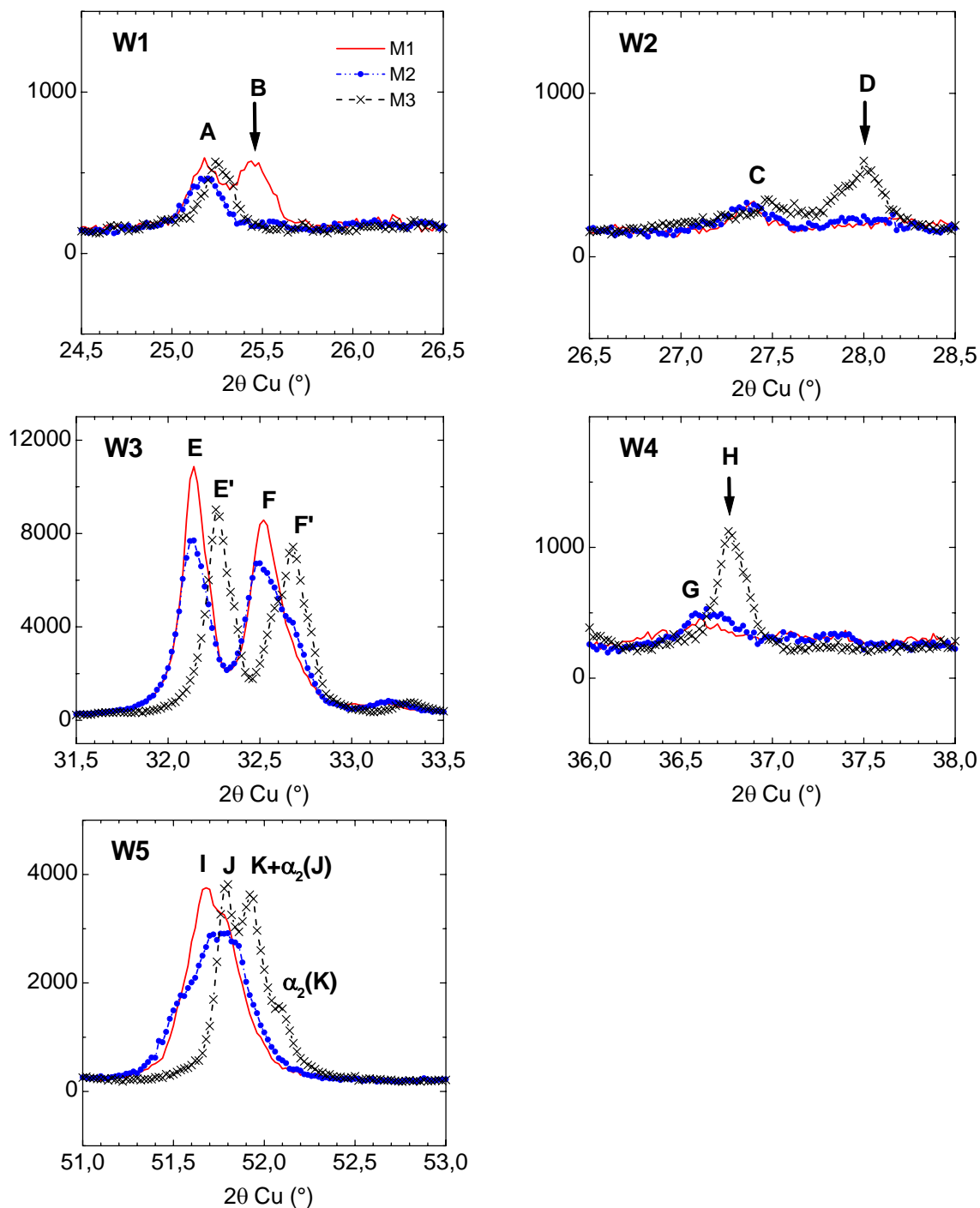


Fig. 2. The five angular windows (W1, W2, W3, W4, W5) useful for the identification of the various polymorphs M1, M2 and M3. The arrows indicate the superstructure Bragg lines. The letters A to K refer to the observed peaks which can be either isolated Bragg lines or group of Bragg lines. The indices are given in Table 2.

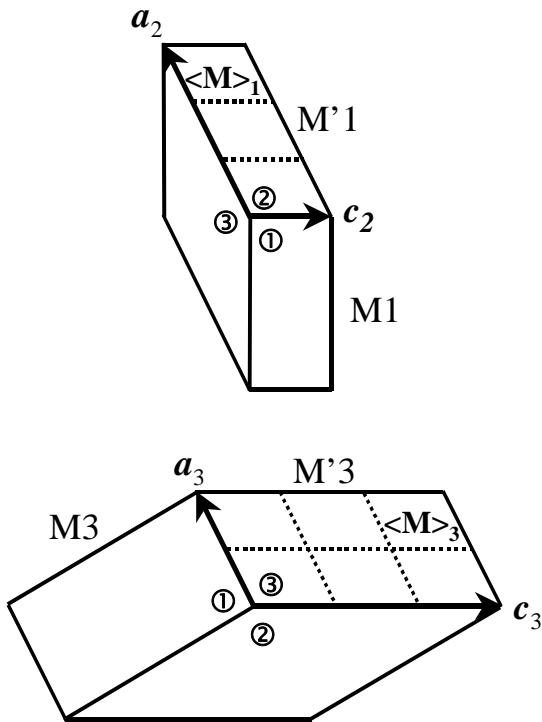


Fig. 3. Relationship between the various equivalent unit cells described in the text.

The figures ① ② ③ are related to the three equivalent choices for the monoclinic unit cells in the monoclinic ( $\mathbf{c}, \mathbf{a}$ ) plane, with the following relations between the unit cell vectors of the three equivalent unit cells:  $\mathbf{c}_2 = \mathbf{a}_1$ ,  $\mathbf{c}_3 = \mathbf{a}_2$ ,  $\mathbf{c}_1 = \mathbf{a}_3$ , and the same  $\mathbf{b}$  unit cell vectors of the three equivalent unit cells.

The dotted lines sketch the superstructure relationship between the  $M_n$  and  $\langle M \rangle_n$  unit cells.

### W3 and W5 windows: identification of the polymorph M1, M2 or M3.

The difference between M1 and M3 polymorphs becomes evident when looking at the W3 and W5 angular windows, which have always been considered in the literature as characteristic of the various polymorphs (Bigare et al. 1967, Guinier and Regourd 1969, Regourd 1979, Qing et al. 1992, Urabe et al. 2002): in both cases, the doublet of Bragg lines is shifted towards the large angles for the M3 alite. However these windows are not able to assess the presence of an eventual superstructure.

As shown by Fig. 1, the diffraction patterns of M1 and M2 alites look very similar. The only significant difference appears in the W3 angular window for the second peak. This peak is made of two Bragg lines: they are merged in M1 diffraction pattern (F) whereas they are separated in the M2 diffraction pattern (F) as well as in the M3 diffraction pattern (F'). As shown by Regourd (Regourd 1979), the inversion of this doublet was already used as a tool to distinguish between the M2 and M3 alite: the pseudo-orthohexagonal indices of the lines are reverted with respect to the M3 alite: 224 and -404 in M2 alite, -404 and 224 in M3

alite. This inversion was related to the (a/b) ratio of the orthohexagonal unit cell parameters:  $a/b < \sqrt{3}$  for M2 alite and  $a/b > \sqrt{3}$  for M3 alite. As shown by Table 3, our (a/b) ratio data are consistent with Regourd data.

### **W1, W2 and W4 windows: identification of the superstructure.**

The M1 and  $\langle M \rangle_1$  structures and the M3 and  $\langle M \rangle_3$  structures can be identified by inspection of the angular windows W1, W2 and W4. Several Bragg lines characteristic of the presence or the lack of superstructure appear in these windows.

The second peak (B) of the doublet of the W1 angular window is characteristic of the M1 structure: it does not exist for the  $\langle M \rangle_1$  structure. The same applies for the W2 and W4 windows: each contains a characteristic Bragg line (D or H) of the M3 structure which does not exist in the  $\langle M \rangle_3$  average structure.

### **Propagation vector for the M3 alite.**

If one now considers the whole diffraction pattern, the stronger superstructure Bragg reflections of M3 alite can be interpreted as satellites of three strong reflections as shown by Fig. 4 and Table 4, which refer to a calculated diffraction pattern of the M'3 superstructure using the single crystal data (Nishi 1985: M3 atomic positions). Almost all the Bragg lines of M3 alite can be interpreted with the propagation vector:

$$\delta \bar{q} = 1/2 \bar{a}^*_{\langle M \rangle_3} - 1/3 \bar{c}^*_{\langle M \rangle_3} \quad (1)$$

by indexing the Bragg lines in the M'3 monoclinic unit cell (choice 3) instead of the conventional M3 unit cell (choice 1). Here  $\bar{a}^*_{\langle M \rangle_3}$  and  $\bar{c}^*_{\langle M \rangle_3}$  are reciprocal unit cell vectors. Within these conventions, six strong superstructure Bragg reflections are found to be the first order satellites of the three Bragg reflections respectively indexed as 300, 200, and 22-6 in the  $\langle M \rangle_3$  unit cell. The W2 and the W4 angular windows contain the two satellites of the 300 Bragg reflection.

Moreover, Urabe et al. (2000, 2002) used a similar -and systematic- approach to interpret the various diffraction patterns in Transmission Electron Microscopy experiments in terms of superstructure of a pseudo-hexagonal subcell. The propagation vector changes from a polymorph to one another.

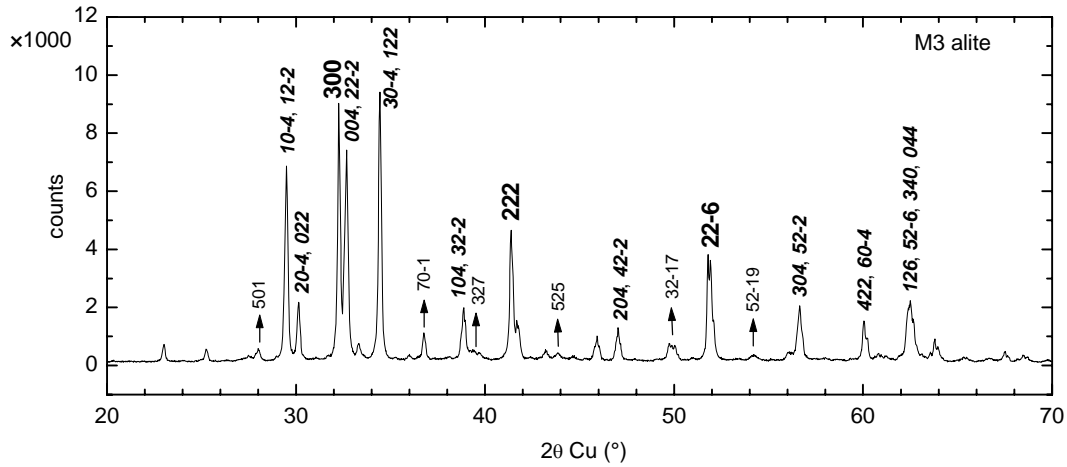


Fig. 4. First order satellite Bragg reflections of the **300**, **222** and **22-6**  $\langle M \rangle_3$  Bragg lines. These satellites, indicated by arrows, are indexed in the  $M'3$  unit cell. The italic indices refer to some of the most important  $\langle M \rangle_3$  Bragg lines.

## 2. Industrial M1 and M3-based clinkers.

The relevance of the five angular windows introduced in the previous paragraph was verified on industrial clinkers.

A systematic analysis of the production of numerous factories of our group made it possible to eliminate the mixtures of polymorphs and choose two characteristic clinkers hereafter referred to as M1-type and M3-type clinker. Following the usual approach used in cement industry, this distinction was based on the examination of the W3 and W5 windows. The chemical composition (wt. %) of these two selected clinkers is given in Table 5. These two samples were ground in a ring mill bowl and were passed through a 40  $\mu\text{m}$  sieve with 0 % retained. The X-Ray diffraction patterns (Figs. 5-7) were registered in the same conditions as alites, except the step counting time of 15s. In order to magnify the weak lines, a square root intensity plot<sup>1</sup> of the region of interest is given in Fig. 6. In these samples, the proportion and the quality of crystallisation of

<sup>1</sup> Several crystallographic residues are used in the Rietveld refinements (Giacovazzo et al. 1995, Rodriguez-Carvajal 1994). The Bragg R-factor  $R_B = \sum_k |I_k^{\text{obs}} - I_k^{\text{calc}}| / \sum_k I_k^{\text{obs}}$  and the crystallographic  $R_F$ -factor  $R_F = \sum_k |F_k^{\text{obs}} - F_k^{\text{calc}}| / \sum_k F_k^{\text{obs}}$  (where  $F = \sqrt{I}$ ) give a good indicator of the quality of the structural model for the strong and the weak Bragg lines respectively. The plot of  $I(2\theta)$  or  $\sqrt{I(2\theta)}$  sketched at Fig. 5 and Fig. 6 can, in the same way, give a visual indicator. The goodness of fit  $\chi^2 = \sum_i w_i (y_{i\text{obs}} - y_{i\text{calc}})^2 / (N-P+C)$  cannot easily be compared between various distinct experiments due to the influence of the weights  $w_i = 1/\sigma_i^2$ .  $N-P+C$  is the number of degrees of freedom of the refinement.  $N$ ,  $P$ ,  $C$  are respectively the number of experimental points of the diffraction pattern, the number of refined parameters, and the number of constraints. The weighted profile factor  $R_{\text{wp}} = [\sum_i w_i (y_{i\text{obs}} - y_{i\text{calc}})^2 / \sum_i w_i y_{i\text{obs}}^2]^{1/2}$  is mainly interesting for the monitoring of the quality of the profile function. Here, the index  $k$  is related to a summation over the Bragg lines and the index  $i$  is related to a summation over the experimental points. Due to the overlapping of the Bragg lines, depending on the profile function, a given experimental point can involve numerous distinct Bragg lines.

belite are higher in M3-type clinker than in M1-type clinker. The structures of belite and aluminate phases are known (Jost et al. 1977, Mondal and Jeffery 1975, Colville and Geller 1972).

Despite the higher complexity of the diffraction patterns due to the additional phases of the clinker (bicalcium silicate, calcium aluminates, - and periclase in M3-type clinker -), the five angular windows remain relevant for the identification of the type and the structure of the polymorph of alite.

The usual W3 and W5 angular windows are similar to that of the synthetic alite, with the same shift of the Bragg line when passing from the M1-type to the M3-type clinker, but some problems in the interpretation may arise from the existence of strong Bragg lines of belite in the W3 angular window (see caption of Fig. 7). Preferential orientation is for a long time known for the E Bragg line due to the pseudo-hexagonal platelet shape of the crystals. It is systematically more important in the clinkers than in the synthetic alites.

In the W2 and W4 angular windows of the M3-type clinker diffraction pattern, one clearly identifies the characteristic Bragg lines (D and H peaks) of the M3 supercell with a small shift due to anisotropic contraction. This clinker is similar to the usual samples described in the literature which almost all exhibit a M3 unit cell. The Mumme (1995) sample with a  $\langle M \rangle_3$  unit cell appears to be special but its existence shows that both  $\langle M \rangle_3$  and M3 can be found in industrial compounds.

Since no supercell peak can be found in the W1 window, the  $\langle M \rangle_1$  alite structure is evidenced for the M1-type sample.

Subsequent Rietveld refinements with  $\langle M \rangle_1$  structural model of alite (de Noirfontaine et al. 2002) for M1-type clinker and M3-type supercell model of alite for M3 clinker were performed (for more details, see de Noirfontaine et al. 2002). The refined unit cell parameters of alites for both clinkers are given in Table 6.

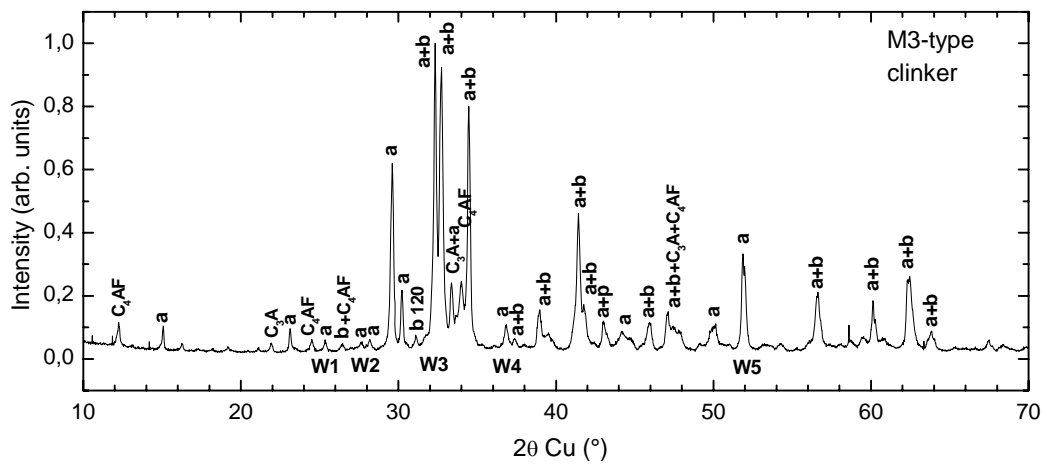
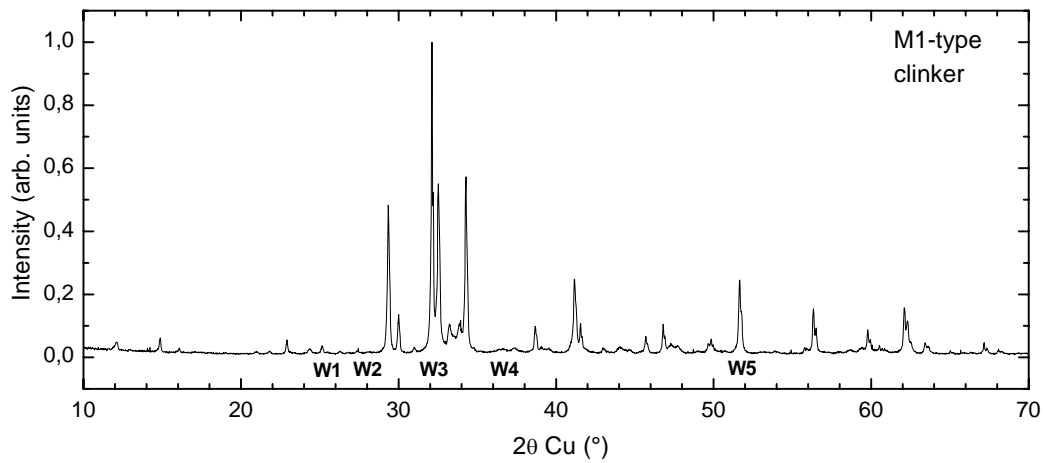
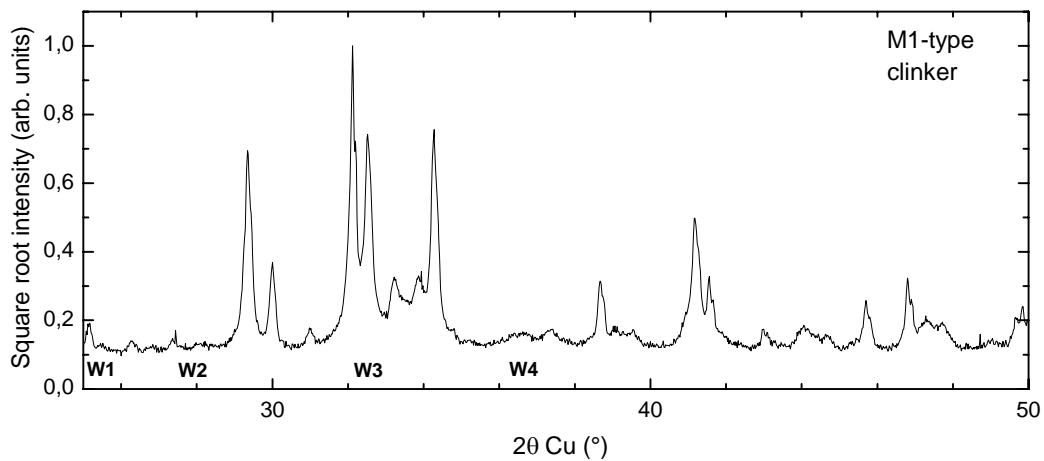


Fig. 5. X-Ray diffraction patterns of industrial clinkers. The letters a, b and p refer to alite, belite and periclase (MgO) Bragg lines. C<sub>3</sub>A and C<sub>4</sub>AF refer to the two aluminate phases with the conventional oxide notations C = CaO, A = Al<sub>2</sub>O<sub>3</sub>, F = Fe<sub>2</sub>O<sub>3</sub>. Alite and belite Bragg lines are overlapping in the quasi-totality of the patterns. The only isolated Bragg line of belite (120) is the weak line isolated at about 31° 2θ<sub>Cu</sub>.



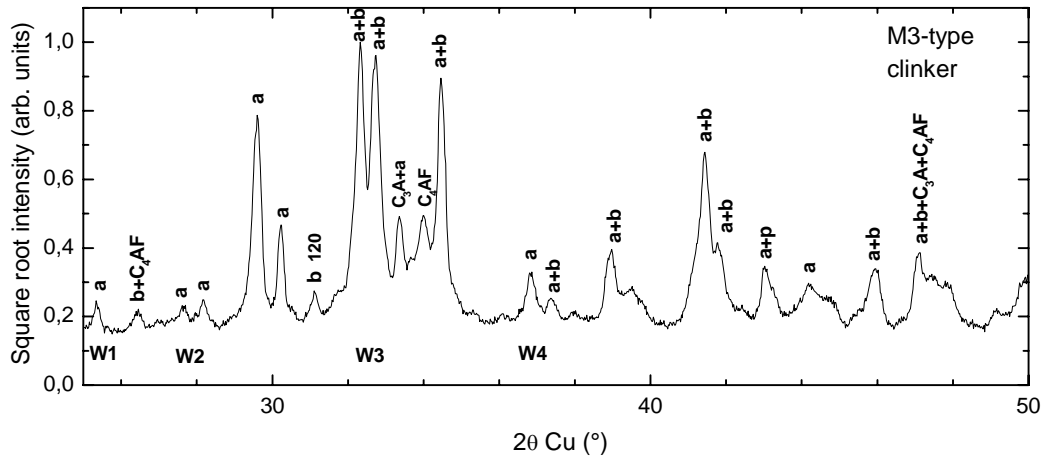
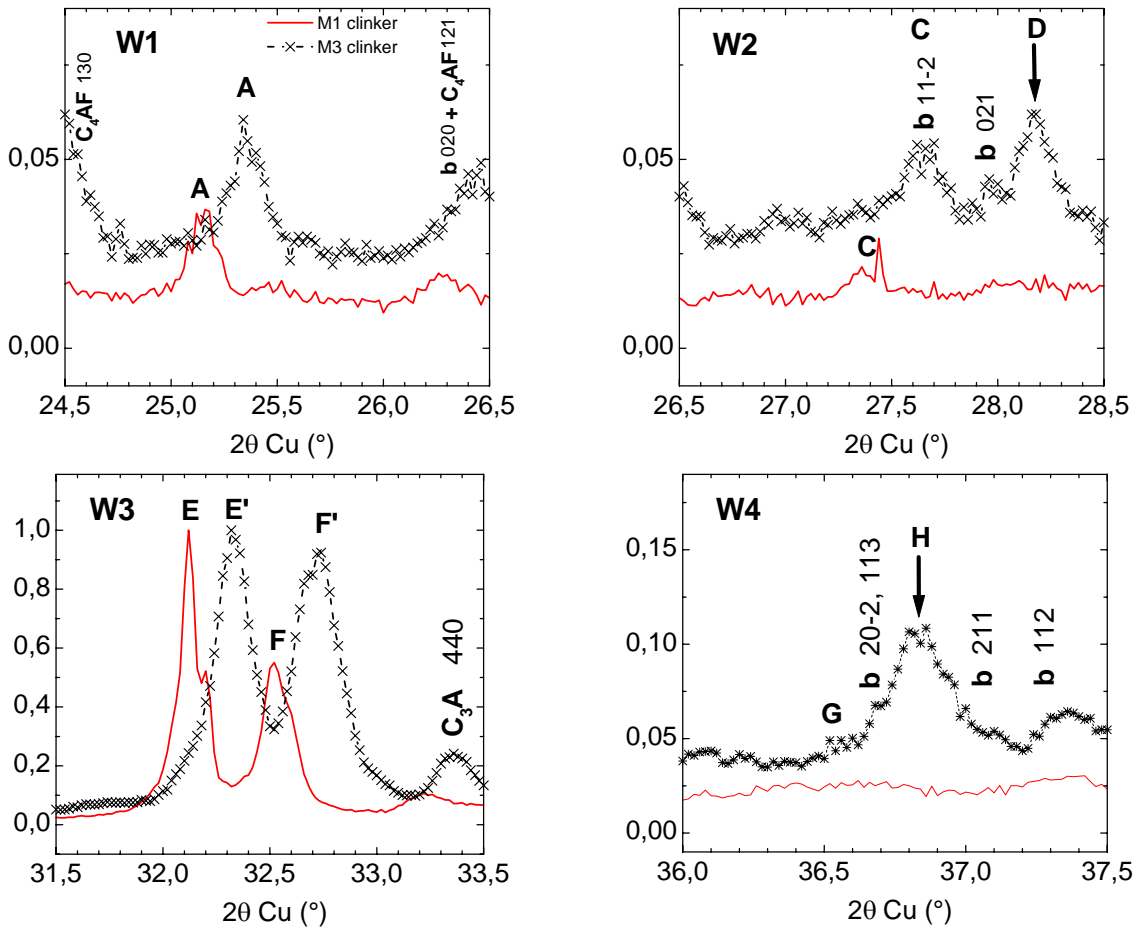


Fig. 6. Same as Fig. 5: the square root intensity plot better evidences the weak Bragg lines.



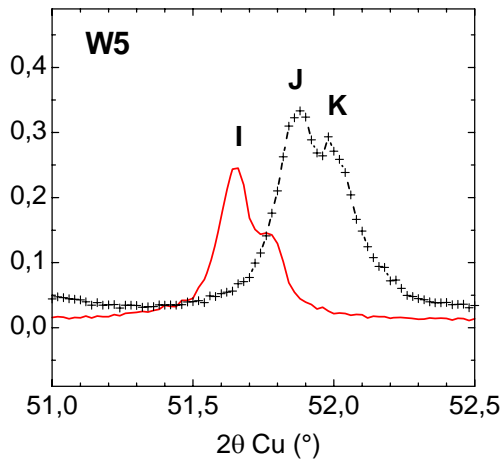


Fig. 7. The five angular windows (W1, W2, W3, W4, W5) useful for the identification of the various polymorphs found in the clinkers. The letter b refers to the belite Bragg lines. In the W3 window, there is a strong overlapping of alite and belite Bragg lines: the E and E' peaks also contain the 10-3, 12-1 and 200 Bragg lines of belite, the F and F' peaks also contain the 022 and 121 Bragg lines of belite. The meaning of the letters is the same as Fig. 2. Due to the unit cell distortions, the A peak of the window W1 appears at distinct angular position for the two types of clinkers.

## Conclusion

Two angular windows ( $W3 = 31.5-33.5^\circ$  and  $W5 = 51-53^\circ 2\theta_{Cu}$ ) in the observed diffraction patterns have traditionally been used to identify the M1 and M3 polymorphs of alite in industrial clinkers. In this paper we show that the examination of three other angular windows ( $W1 = 24.5-26.5^\circ$ ,  $W2 = 26.5-28.5^\circ$ , and  $W4 = 36-38^\circ 2\theta_{Cu}$ ) is also relevant for the identification of presence of superstructure effects and makes it possible to distinguish directly and visually between the four  $\langle M \rangle_1$ , M1,  $\langle M \rangle_3$ , M3 models for use in subsequent Rietveld analysis (see also de Noirfontaine et al. 2002).

The two M3 and  $\langle M \rangle_3$  structures have been observed in the M3-type clinkers. We find only a  $\langle M \rangle_1$  unit cell in our M1-type samples. But the M1 unit cell, observed in the synthetic alite, may also be observed.

## References

- Bigare, M., Guinier, A., Mazieres, C., Regourd, M., Yannaquis, N., Eysel, W., Hahn, T., and Woermann, E. (1967). "Polymorphism of Tricalcium Silicate and its Solid Solutions", *J. Am. Ceram. Soc.* 50 (11), 609-619.
- Colville, A.A. and Geller, S. (1972). "The Crystal Structure of  $Ca_2Fe_{1.43}Al_{0.57}O_5$  and  $Ca_2Fe_{1.28}Al_{0.72}O_5$ ", *Acta Cryst.* B28, 3196-3200.

de Noirfontaine, M.-N., "Etude structurale et cristallographie du composé majoritaire du ciment anhydre : le silicate tricalcique", PhD thesis, January 2000, Ecole Polytechnique, France.

de Noirfontaine, M.-N., Courtial, M., Dunstetter, F., Gasecki, G., and Signes-Frehel, M., "Modelling of Alite, an Industrial Challenge: The Major Compound of Anhydrous Portland Cement Revisited", *Cem. Conc. Res.*, submitted (2002).

Jost, K.H., Ziemer, B., and Seydel, R. (1977). "Redetermination of the structure of  $\beta$ -Dicalcium Silicate", *Acta Cryst.* B33, 1696-1700.

Giacovazzo, C., Monaco, H.L., Viterbo, D., Scordari, F., Gilli, G., Zanotti, G. and Catti, M. (1995), *Fundamentals of Crystallography*, chapter 2, 111, Ed. C. Giacovazzo, Oxford University Press.

Guinier, A., and Regourd, M. (1969). "Structure of Portland Cement Minerals", *Proc. of the 5th ISCC*, Tokyo, Vol. 1, 1-41.

*International Tables for Crystallography*, Vol. A, chapter 2, 35-38, Ed. Theo Hahn, Kluwer Academic Publisher, 1995.

Larson, A.C., and Von Dreele, R.B. (1988), "GSAS General Structure Analysis System", *Operational Manual*, Los Alamos National Laboratory LAUR 86-748.

Maki, I., and Goto, K. (1982). "Factors Influencing the Phase Constitution of Alite in Portland Cement Clinker", *Cem. Conc. Res.* 12, 301-308.

Mondal, P. and Jeffery, J.W. (1975). "The Crystal Structure of Tricalcium Aluminate,  $\text{Ca}_3\text{Al}_2\text{O}_6$ ", *Acta Cryst.* B31, 689-696.

Mumme, W.G. (1995). "Crystal Structure of Tricalcium Silicate from a Portland Cement Clinker and its Application to Quantitative XRD Analysis", *N. Jb. Miner. Mh. H.* 4, 145-160.

Nishi, F., Takeuchi, Y., and Maki, I. (1985). "The Tricalcium silicate  $\text{Ca}_3\text{O}[\text{SiO}_4]$ : the Monoclinic Superstructure", *Zeit. Krist.* 172, 297-314.

Qing, Y., Jianmin, K., and Baoyuan, L. (1992). "Effect of Fluorite-Gypsum Composite Mineralizer on the Microstructure and Properties of Portland Cement Clinker Phase", *Proc. of the 9th ICCG, New Delhi*, 2, 342-350.

Regourd, M. (1970). "Cristallographie des constituants du clinker de ciment Portland", *Bull. Liais. Labo. Routiers N° spécial 0*, 58-73.

Regourd, M. (1979). "Polymorphisme du silicate tricalcique. Nouvelles données de la diffraction des rayons X", *C. R. Acad. Sc. Paris t. 289*, 17-20.

Rietveld, H.M. (1969). "A profile refinement method for nuclear and magnetic structures", *J. Appl. Crystallogr.* 2, 65-71.

Rodriguez-Carvajal J. (1994). Note prepared for the Nordic Research Course "The Rietveld Method in Practice: the program FULLPROF".

Urabe, K., Shirakami, T., and Iwashima, M. (2000). "Superstructure in a Triclinic Phase of Tricalcium Silicate", *J. Am. Ceram. Soc.* 83 (5), 1253-1258.

Urabe, K., Nakano, H., and Morita, H. (2002). "Structural modulations in Monoclinic Tricalcium Silicate Solid Solutions Doped with Zinc Oxyde, M(I), M(II), and M(III)", *J. Am. Ceram. Soc.* 85 (2), 423-29.

Table 1. Chemical analysis (wt. %) for the three synthetic alites.

Alite	M1	M2	M3
Ig. loss	0.42	0.59	0.12
CaO	70.48	70.85	70.86
SiO <sub>2</sub>	24.47	25.21	25.73
Al <sub>2</sub> O <sub>3</sub>	1.05	1.13	1.02
Fe <sub>2</sub> O <sub>3</sub>	1.05	1.08	—
MgO	0.99	1.06	2.18
SO <sub>3</sub>	1.55	0.07	0.09

Table 2. Indices of the Bragg lines of Fig. 2 -or group of Bragg lines- within the various structural models described in the text and sketched at Fig. 3. The five angular windows used to discriminate between the various monoclinic polymorphs of alite are: W1 = 24.5 - 26.5°, W2 = 26.5 - 28.5°, W3 = 31.5 - 33.5°, W4 = 36.0 - 38.0°, W5 = 51.0 - 53.0° ( $2\theta_{Cu}$  range). The pseudo-hexagonal unit cells OH<sub>1</sub> to OH<sub>3</sub> used by Regourd (Bigare et al. 1967, Guinier et al. 1969, Regourd 1979) and co-workers are very similar to the M1 unit cell, with reverted a and c unit cell vectors. Each letter refers to a given observed peak in the X-Ray diffraction pattern. We just consider here the strongest diffraction lines arising from the Rietveld analysis of the data. The neglected components are much weaker.

		M1 alite				M3 alite				M2 alite		
		M1	M'1	<M> <sub>1</sub>	OH <sub>1</sub>			M3	M'3	<M> <sub>3</sub>	OH <sub>3</sub>	OH <sub>2</sub>
W1	A	-3 1 0	3 1 -3	1 1 -3	3 1 0	A	7 1 2	2 1 -9	1 1 -3	3 1 0		
	B	-3 1 1	2 1 -3	-	3 1 -1	A	0 2 0	0 2 0	0 2 0	0 2 0		
	B	-3 1 -1	4 1 -3	-	3 1 1							
W2	C	0 2 -3	3 2 0	1 2 0	0 2 3	C	-9 1 0	0 1 9	0 1 3	-3 1 3		
						C	-9 1 1	1 1 8	-	-		
						C	-2 2 2	2 2 0	1 2 0	0 2 3		
						D	10 0 1	1 0 -11	-	-		
						D	-6 0 5	5 0 1	-	-		
W3	E	0 0 -9	9 0 0	3 0 0	0 0 9	E'	-6 0 6	6 0 0	3 0 0	0 0 9	0 0 9	
	F	4 0 -4	0 0 4	0 0 4	-4 0 4	F'	-12 0 0	0 0 12	0 0 4	-4 0 4	2 2 4	
	F	-2 2 -4	6 2 -2	2 2 -2	2 2 4	F'	2 2 4	4 2 -6	2 2 -2	2 2 4	-4 0 4	
W4	G	-4 1 -5	9 1 -4	3 1 -4	4 1 5	H	-6 0 7	7 0 -1	-	-		
W5	I	-6 2 0	6 2 -6	2 2 -6	6 2 0	J	14 2 4	4 2 -18	2 2 -6	6 2 0		
	J	0 4 0	0 4 0	0 4 0	0 4 0	K	0 4 0	0 4 0	0 4 0	0 4 0		

Table 3. Rietveld refinements of the various polymorphs. Structural models used were those of de Noirfontaine (2000) and Nishi et al. (1985) for M1 and M3 superstructures. No structural model is known for M2 alite: the atomic positions of the average  $\langle M \rangle_1$  unit cell (de Noirfontaine 2000) were used and refined, with a treatment of the silicate tetrahedra as rigid bodies.

The unit cells without experimental errors are computed using transformation matrices. The  $(a/b)_{OH}$  ratio is related to the discussion of Regourd (1979) allowing the discussion between the M2 and M3 polymorphs.

Sample	Unit cell	a (nm)	b (nm)	c (nm)	$\beta$ (deg.)	V(nm <sup>3</sup> )	space group	$(a/b)_{OH}$
<b>M1 alite</b> <b>our data</b>	<b>M'1</b> choice 2 $\langle M \rangle_1$	2.78736(2)	0.70590(5)	1.22575(8)	116.030(6)	2.167	Pc	
		0.92912	0.7059	1.22575	116.03	0.7224	Pc	
	OH1 $\equiv$ M1	1.22575	0.7059	2.50462	90.06	2.167		
		$R_B = 9.1$	$R_F = 7.8$	$\chi^2 = 8.32$	$R_{wp} = 19.1$			
<b>M2 alite</b> <b>our data</b>	$\langle M \rangle_2$	0.92963(5)	0.70823(4)	1.22023(7)	116.114(4)	0.7214	?	
	OH <sub>2</sub>	1.22023	0.70823	2.50421	89.83	2.164	?	1.7229
		$R_B = 8.2$	$R_F = 8.6$	$\chi^2 = 6.23$	$R_{wp} = 17.4$			
<b>M3 alite</b> <b>our data</b>	<b>M'3</b> choice 3	1.85179(10)	0.70330(4)	3.6694(19)	116.038(4)	4.294	Im	
	M3 choice 1	3.30577	0.70330	1.85179	94.18	4.294	Cm	
	$\langle M \rangle_3$	0.9259	0.7033	1.22313	116.04	0.7156	Am	
	OH <sub>3</sub>	1.22313	0.7033	2.49573	90.09	2.147		1.7391
		$R_B = 14$	$R_F = 14$	$\chi^2 = 9.54$	$R_{wp} = 22.1$			
Regourd data	OH <sub>2</sub>	1.2333	0.7137	2.5442	90	2.239		1.728
	OH <sub>3</sub>	1.2372	0.7123	2.5440	90	2.242		1.737
Mumme data	Powder sample	1.22078(10)	0.70930(6)	0.93062(9)	116.115(6)	0.7211	Cm	
	Single crystal	1.2235(3)	0.7073(2)	0.9298(3)	116.31(5)	0.7213	Cm	

Table 4. Examples of some superstructure Bragg reflections interpreted as first order satellites of the  $\langle M \rangle_3$  structure reflections with the  $\delta \bar{q}$  propagation vector. The first lines of the table must be read as follows: the 1 0 -11 and 3 0 -13 superstructure reflections are the first order satellites of the 1 0 -4  $\langle M \rangle_3$  Bragg reflection.

$2\theta_{Cu}$ (deg.)	$d(\text{\AA})$	hkl ( M3)	hkl (M'3)	n	hkl $\langle M \rangle_3$
27.81	3.205	10 0 1	1 0 -11	-1	1 0 -4
31.68	2.822	10 0 3	3 0 -13	+1	
28.12	3.170	4 2 1	1 2 -5	-1	1 2 -2
31.67	2.830	4 2 3	3 2 -7	+1	
28.15	3.174	6 0 -5	5 0 1	-1	3 0 0
36.75	2.449	6 0 -7	7 0 -1	+1	
29.93	2.983	2 2 3	3 2 -5	-1	2 2 -2
35.92	2.498	2 2 5	5 2 -7	+1	
30.09	2.967	6 0 5	5 0 -11	-1	3 0 -4
38.89	2.313	6 0 7	7 0 -13	+1	
33.59	2.665	-8 2 1	1 2 7	-1	1 2 2
35.93	2.497	-8 2 3	3 2 5	+1	
39.46	2.282	-10 2 3	3 2 7	-1	2 2 2
43.77	2.066	-10 2 5	5 2 5	+1	
49.69	1.833	14 2 3	3 2 -17	-1	2 2 -6
54.32	1.687	14 2 5	5 2 -19	+1	

Table 5. Chemical analyses (wt. %) for the M1 and M3-type clinkers.

Clinker	M1-type	M3-type
Ig. loss	0.34	0.56
CaO	67.54	63.83
SiO <sub>2</sub>	21.16	21.20
Al <sub>2</sub> O <sub>3</sub>	5.03	4.98
Fe <sub>2</sub> O <sub>3</sub>	3.78	3.16
MgO	0.76	3.76
SO <sub>3</sub>	0.88	1.23
K <sub>2</sub> O	0.13	0.72
TiO <sub>2</sub>	0.23	0.24
Na <sub>2</sub> O	0.07	0.13
P <sub>2</sub> O <sub>5</sub>	0.03	0.07
SrO	0.02	0.11
MnO	0.03	0.03

Table 6. The unit cell parameters for alite in each clinker sample, with the same convention as that used in Table 3.

Clinker	Unit cell	a (nm)	b (nm)	c (nm)	$\beta$ (deg.)	V(nm <sup>3</sup> )	space group	(a/b) <sub>OH</sub>
M1-type	Alite <M> <sub>1</sub>	0.92989(6)	0.70801(4)	1.22484(6)	116.051(6)	0.72447	Pc	
	OH <sub>1</sub>	1.22484	0.70801	2.50625	89.99	2.1734		
M3-type	Alite M'3	1.85321(1)	0.70415(4)	3.67339(2)	116.086(6)	4.3052	Im	1.739
	M3	3.30777	0.70415	1.85321	94.125	4.3052	Cm	
	<M> <sub>3</sub>	0.92660	0.70415	1.22446	116.086	0.71754	Am	
	OH <sub>3</sub>	1.22446	0.70415	2.49695	90.05	2.1526		